H−X Bond Activation via Hydrogen Transfer to Hydride in Ruthenium N-Heterocyclic Carbene Complexes: Density Functional and Synthetic Studies

Sarah L. Chatwin,[†] Matthew G. Davidson,[§] Cheryl Doherty,[§] Steven M. Donald,[‡] Rodolphe F. R. Jazzar,[†] Stuart A. Macgregor,*[,‡] Garry J. McIntyre,[#] Mary F. Mahon,*[,§] and Michael K. Whittlesey*[,†]

School of Engineering and Physical Sciences, Heriot-Watt University, Edinburgh, EH14 4AS, U.K., Department of Chemistry, University of Bath, Claverton Down, Bath BA2 7AY, U.K., X-ray Crystallographic Unit, Department of Chemistry, University of Bath, Claverton Down, Bath BA2 7AY, U.K., and Institut Laue-Langevin, BP156, 38042 Grenoble Cedex 9, France

Received August 29, 2005

The reactions of *tcc*-Ru(IMes)$_2$(AsPh$_3$)(CO)H$_2$ (**1**, IMes = bis(1,3-(2,4,6-trimethylphenyl)imidazol-2-ylidene)) with HX substrates (X = OH, OEt, SH, S^{n}Pr) have been reinvestigated and shown to lead directly to the formation of the 16-electron species Ru(IMes)$_2$(CO)(X)H (**4-X**). The fluoro analogue Ru(IMes)$_2$(CO)(F)H (**4-F**) has also been synthesized, and X-ray and neutron diffraction studies show that this exhibits a square-pyramidal geometry with hydride in the axial site. Density functional calculations have been performed on one possible mechanism for the formation of **4-X** from **1** with various HX (X = F, Cl, OH, SH, NH$_2$, PH$_2$, CH$_3$, and SiH$_3$), involving initial AsPh$_3$/HX substitution followed by H-transfer to hydride and H$_2$ loss. With X = SH, H-transfer in both *tcc*-Ru(IMes)$_2$(CO)(H$_2$S)(H)$_2$ and *ttt*-Ru(IMes)$_2$(CO)(H$_2$S)(H)$_2$ was considered and shown to be kinetically accessible and thermodynamically favored, suggesting that such dihydrides should not be stable with respect to this step. The calculations indicate that the ease of formation of **4-X** becomes more kinetically and thermodynamically favored according to the trends F > OH > NH$_2$ > CH$_3$ and Cl > SH > PH$_2$ < SiH$_3$, with the reactions of second-row HX substrates being more favored than the first-row analogues. Calculated reaction exothermicities allow the derivation of relative Ru−X bond strengths in **4-X**, and comparison with experimentally determined M−X relative bond strengths in the literature highlights the importance of X → M π-donation in determining trends in M−X bond dissociation energies in unsaturated systems.

Introduction

We have recently described the reactivity of the bis-N-heterocyclic carbene complex *tcc*-Ru(IMes)$_2$(AsPh$_3$)(CO)H$_2$, **1**, with HX (IMes = bis-1,3-(2,4,6-trimethylphenyl)imidazol-2-ylidene; X = OH, OEt, SH, S^{n}Pr) to afford species with Ru−X bonds.[1] We postulated that the reaction of **1** with HX proceeded via initial AsPh$_3$ substitution, with rearrangement giving the *trans*-dihydride *ttt*-Ru(IMes)$_2$(CO)(HX)H$_2$ (***trans*-2-X**, see Scheme 1). Subsequent hydrogen-transfer (abbreviated from now on as H-transfer) would yield the dihydrogen intermediate Ru(IMes)$_2$(CO)(X)(η^2-H$_2$)(H) (***trans*-3-X**), which upon H$_2$ dissociation would lead to Ru(IMes)$_2$(CO)(X)H (**4-X**). **4-X** are 16-electron (16e) unsaturated species and exhibit a range of reactions including ligand addition (e.g., with CO to give *tcc*-Ru(IMes)$_2$(CO)$_2$(X)H, **5-X**), various small molecule insertions, and H-transfer processes.

H-transfer processes of the type linking ***trans*-2-X** and ***trans*-3-X** above have been invoked to explain H/D scrambling processes in a range of M(HX)(H) complexes (HX = NH$_3$[2]/amines,[3] H$_2$O[4]/alcohols,[5] and H$_2$S[6]/thiols[7]). The equilibrium usually lies to the left, although Morris has been able to directly observe the hydrido-thiol [Os(PPh$_3$)$_2$(CO)(quS-H)(H)]$^+$ in equilibrium with the dihydrogen thiolate [Os(PPh$_3$)$_2$(CO)(quS)(η^2-H$_2$)]$^+$ (quS = quinoline-8-thiolate).[7c] The diverse range of metal/ligand combinations cited above has meant that, to date, there has been no systematic study of the factors that control HX bond activation via this type of H-transfer. The H-transfer

* Corresponding author. E-mail: s.a.macgregor@hw.ac.uk.
‡ Heriot-Watt University.
† Department of Chemistry, University of Bath.
§ X-ray Crystallographic Unit, University of Bath.
# Institut Laue-Langevin.

(1) (a) Jazzar, R. F. R.; Bhatia, P. H.; Mahon, M. F.; Whittlesey, M. K. *Organometallics* **2003**, *22*, 670. (b) Chatwin, S. L.; Diggle, R. A.; Jazzar, R. F. R.; Macgregor, S. A.; Mahon, M. F.; Whittlesey, M. K. *Inorg. Chem.* **2003**, *42*, 7695.

(2) (a) Koelliker, R.; Milstein, D. *J. Am. Chem. Soc.* **1991**, *113*, 8524. (b) Holland, A. W.; Bergman, R. G. *J. Am. Chem. Soc.* **2002**, *124*, 14684.

(3) (a) Fryzuk, M. D.; Montgomery, C. D.; Rettig, S. J. *Organometallics* **1991**, *10*, 467. (b) Abdur-Rashid, K.; Lough, A. J.; Morris, R. H. *Organometallics* **2000**, *19*, 2655. (c) Sandoval, C. A.; Ohkuma, T.; Muñiz, K.; Noyori, R. *J. Am. Chem. Soc.* **2003**, *125*, 13490. (d) Dahlenburg, L.; Gotz, R. *Eur. J. Inorg. Chem.* **2004**, 888.

(4) (a) Crabtree, R. H.; Lavin, M.; Bonneviot, L. *J. Am. Chem. Soc.* **1986**, *108*, 4032. (b) Leoni, P.; Sommovigo, M.; Pasquali, M.; Midollini, S.; Braga, D.; Sabatino, P. *Organometallics* **1991**, *10*, 1038.

(5) (a) Albeniz, A. C.; Heinekey, D. M.; Crabtree, R. H. *Inorg. Chem.* **1991**, *30*, 3632. (b) Sung, K.-M.; Huh, S.; Jun, M.-J. *Polyhedron* **1998**, *18*, 469.

(6) (a) Sellmann, D.; Käppler, J.; Moll, M. *J. Am. Chem. Soc.* **1993**, *115*, 1830. (b) Sellmann, D.; Rackelmann, G. H.; Heinemann, F. W. *Chem. Eur. J.* **1997**, *3*, 2071. (c) Schwarz, D. E.; Dopke, J. A.; Rauchfuss, T. B.; Wilson, S. R. *Angew. Chem., Int. Ed.* **2001**, *40*, 2351. (d) Sellmann, D.; Prakash, R.; Heinemann, F. W.; Moll, M.; Klimowicz, M. *Angew. Chem., Int. Ed.* **2004**, *43*, 1877.

(7) (a) Jessop, P. G.; Morris, R. H. *Inorg. Chem.* **1993**, *32*, 2236. (b) Schlaf, M.; Morris, R. H. *J. Chem. Soc., Chem. Commun.* **1995**, 625. (c) Schlaf, M.; Lough, A. J.; Morris, R. H. *Organometallics* **1996**, *15*, 4423.

10.1021/om0507427 CCC: $33.50
Publication on Web 11/23/2005

Scheme 1

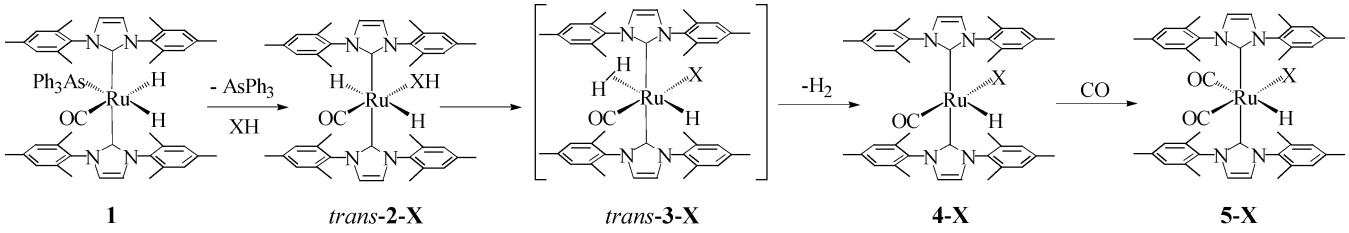

reactions of the type shown in Scheme 1 therefore provide us with a unique opportunity to assess the role of X in controlling this process.

We report here the results of our experimental and computational investigations into the H-transfer reactions of **1** with H_2O and H_2S, the extension of the experimental studies to the analogous reaction with HF, and our computational studies on a wider range of HX substrates. The results of our initial study into H-transfer in ***trans*-2-SH** are first described, and these show that *trans*-dihydride species of this type are in fact unstable with respect to H-transfer. On this basis we have reconsidered the characterization of structures based on ***trans*-2-X** and found them to be 16e $Ru(IMes)_2(CO)(X)H$ complexes of type **4-X**. This finding is supported by X-ray and neutron diffraction studies on $Ru(IMes)_2(CO)(F)H$ (**4-F**). Consequently, we have considered an alternative mechanism for the reaction of HX species with **1** that involves simple $AsPh_3$/HX substitution followed by H-transfer from the *cis*-dihydrides ***cis*-2-X**.[8] Our computational studies on this process are described for X = F, Cl, OH, SH, NH_2, PH_2, CH_3, and SiH_3.[9]

Results and Discussion

H-Transfer in *ttt*-$Ru(IMes)_2(CO)(H_2S)H_2$ (*trans*-2-SH). We have previously reported a computed structure for *ttt*-$Ru(IMes)_2(CO)(H_2S)H_2$ (***trans*-2-SH**)[1b] and its model complex *trans*-$Ru(IH)_2(CO)(H_2S)H_2$ (***trans*-2′-SH**, where IH = imidazol-2-ylidene), and reactivity studies were initiated on the latter. H-transfer from the SH_2 ligand in ***trans*-2′-SH** to a neighboring hydride was computed to be extremely facile, with an activation barrier of only 3.6 kcal/mol (Figure 1). The H-transfer transition state requires the Ru−S distance to lengthen from 2.46 Å to 2.64 Å in order to reorientate the SH_2 ligand and present one hydrogen toward the accepting hydride. In contrast, the S−H bond to be cleaved is barely affected at this stage. The product of H-transfer, the dihydrogen complex $Ru(IH)_2(CO)(HS)(\eta^2\text{-}H_2)H$ (***trans*-3′-SH**), is calculated to be 27.8 kcal/mol more stable than ***trans*-2′-SH** and features a conventional dihydrogen ligand (H−H = 0.84 Å) lying parallel to the IH−Ru−IH axis. H-transfer is also accompanied by a reorientation of the IH ligands, which are initially parallel to the H−Ru−H axis in ***trans*-2′-SH**, but rotate to form H-bonding contacts with the hydrosulfido ligand in ***trans*-3′-SH** (N−H···S = 2.35 Å). This feature must arise from the use of IH ligands in our model, and in order to assess how this affects the energetics of H-transfer, we have repeated our study using hybrid QM/MM calculations on ***trans*-2-SH** itself.

In the QM/MM approach a model molecule is partitioned into layers to which different computational approaches can be applied (Scheme 2). In our calculations, all mesityl groups are described at a molecular mechanics level, while a density functional method is retained for all other atoms (see below for ***trans*-2-SH**; full details are given in the Experimental Section).

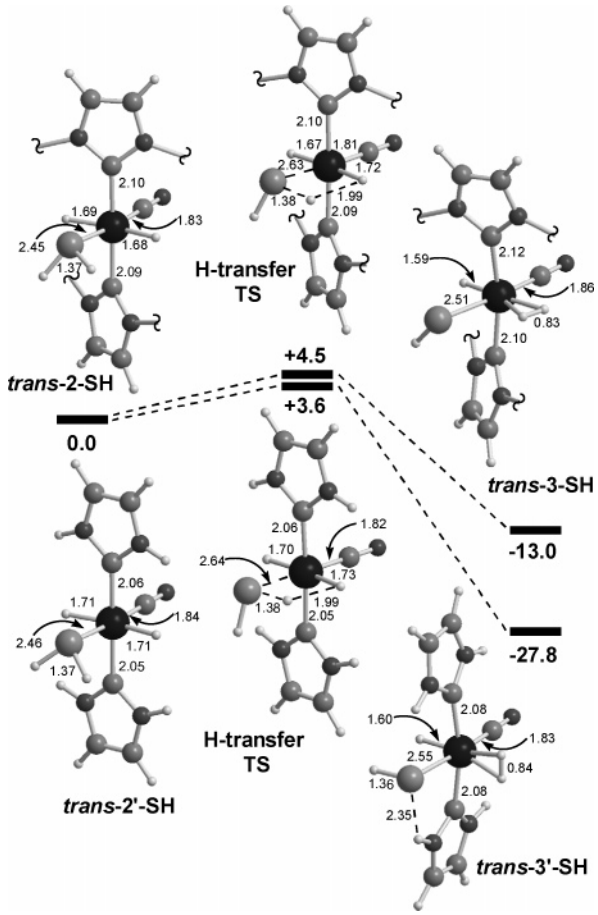

Figure 1. Computed reaction profiles (kcal/mol) for H-transfer in *trans*-$Ru(IR)_2(CO)(H_2S)H$ (R = H, ***trans*-2′-SH**; R = Mes, ***trans*-2-SH**). Key distances are given in Å, and structures for the IMes model are truncated at the N−Mes bonds for clarity.

(8) Other mechanisms may be proposed for the reaction of **1** with HX species to form **4-X** and H_2. For example, protonation of **1** by HX to form $[Ru(IMes)_2(AsPh_3)(CO)(\eta^2\text{-}H_2)H]^+X^-$ followed by $AsPh_3/X^-$ substitution will result in the formation of the same intermediate ***cis*-3-X**. In addition, a referee suggested that HX may facilitate the formation of an unsaturated Ru center by trapping free $AsPh_3$ as $[AsPh_3H]^+$. Unfortunately the reaction of **1** with HX is so rapid that it has not been possible to probe experimentally the mechanism of these reactions in any further detail,[1] and we focus here on the $AsPh_3$/HX substitution−H-transfer mechanism in order to highlight the factors controlling the H-transfer step.

(9) We are aware of only one previous theoretical study that has addressed the addition of H−X over a L_nM−H bond to give an $L_nM(X)(\eta^2\text{-}H_2)$ species. For the reaction of *trans*-$Pd(NH_3)(H)_2(H_2O)$ a barrier of 13 kcal/mol was computed via MP2 calculations, and the H-transfer step to form $Pd(NH_3)(H)(\eta^2\text{-}H_2)(OH)$ is downhill by 2 kcal/mol. See: Milet, A.; Dedieu, A.; Kapteijn, G.; van Koten, G. *Inorg. Chem.* **1997**, *36*, 3223. The base-assisted heterolytic cleavage of the η^2-H_2 ligand in *cis*-$Rh(PH_3)_2(\eta^2\text{-}H_2)(HCO_2)$ has also been studied computationally: Hutschka, F.; Dedieu, A. *J. Chem. Soc., Dalton Trans.* **1997**, 1899.

Scheme 2

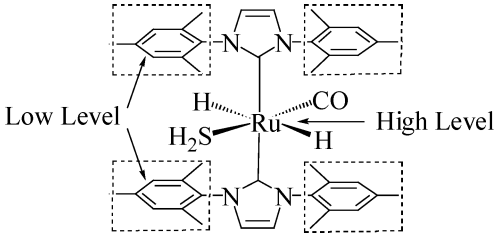

An H-transfer reaction profile based on our previously optimized structure of ***trans*-2-SH** allowed us to locate a transition state with a calculated activation barrier of 4.5 kcal/mol, which led directly to $Ru(IMes)_2(CO)(HS)(\eta^2\text{-}H_2)H$ (***trans*-3-SH**, $E = -13.0$ kcal/mol). The geometries located with the two model systems are very similar in terms of the ligands participating in H-transfer, and any differences elsewhere can be ascribed to the bulk of the IMes ligands. This results in lengthening of all $Ru-C_{NHC}$ distances by ca. 0.04 Å and a staggered arrangement of the two IMes ligands over the H−Ru−H axis in ***trans*-2-SH**. This arrangement is also seen in the H-transfer transition state and is now retained in ***trans*-3-SH**, the deviation from coplanarity of the imidazole rings being in the range 35−48° throughout. With IMes there are no possible H-bonding interactions to drive the NHC ligand rotation that was computed in ***trans*-3′-SH**. For the same reason, the S−H bond in ***trans*-3-SH** can now lie out of the equatorial plane.

The barrier for H-transfer is very similar in both model systems, but the overall energy change for this process is significantly less favorable with IMes. The stability of the dihydrogen complex therefore appears to be overestimated with IH, due to the neglect of steric effects, the introduction of N−H···S H-bonding interactions, or a combination of both. The energetics of H-transfer are therefore sensitive to the nature of the NHC model ligand. However, even with IMes, H-transfer is computed to be both kinetically easily accessible and thermodynamically favorable. In turn, this suggests that *trans*-dihydride structures such as ***trans*-2-X** ought not to be stable with respect to H-transfer. Consequently, we have reassessed our previous interpretation concerning the structure of ***trans*-2-SH** and its oxygen-based analogues ***trans*-2-OH** and ***trans*-2-OEt**.

Recharacterization of *trans*-2-X (X = SH, OH, OEt). The experimental assignment of compounds ***trans*-2-X** (X = SH, OH, OEt) was uniformly based on $^1H/^{13}C\{^1H\}$ NMR spectroscopy and X-ray diffraction.[1] However, the X-ray data for both ***trans*-2-SH** and ***trans*-2-OEt** showed 1:1 positional disorder in the EtOH/CO and H_2S/CO ligands, which precluded us from determining accurate Ru−O and Ru−S distances. In addition, we were unable to reliably locate the O-H_2, EtO-*H*, and HS-*H* hydrogen atoms. In light of the results of the DFT calculations described above highlighting the propensity of ***trans*-2-X** species to undergo H-transfer, additional experiments were undertaken that indicate that these species are in fact 16e $Ru(IMes)_2(CO)(OH)H$ (**4-OH**), $Ru(IMes)_2(CO)(OEt)H$ (**4-OEt**), and $Ru(IMes)_2(CO)(SH)H$ (**4-SH**).[10] The most convincing evidence for this presents itself in the form of two low-field *doublet* (and not triplet) resonances for the carbene and carbonyl signals in the $^{13}C-^1H$ coupled NMR spectra, proving the existence of a single hydride ligand.[11] Further verification arose from recording proton NMR spectra on these **4-X** systems with a long pulse delay (10 s), which afforded integral ratios of 1:36 for the RuH:IMes methyl signals and 1:4 for RuH:NC*H*=NC*H* resonances. With hindsight, the high-field hydride chemical shifts that we presented as evidence for a *trans*-dihydride geometry[12] are also fully consistent with five-coordinate structures with hydride *trans* to a vacant site.[13] The IR carbonyl bands of **4-X** (1861, 1886, 1879 cm^{-1} for X = OH, OEt, and SH, respectively) are close in frequency to that found for the 16e complex $Ru(IMes)_2(CO)(F)H$ (**4-F**; 1873 cm^{-1}) discussed below and are similar to those reported by Caulton and co-workers for a range of analogous $Ru(P^tBu_2Me)_2(CO)(X)H$ compounds, where X is a π-donor ligand.[13b,c,14]

Formation, Characterization, and Reactivity toward CO of $Ru(IMes)_2(CO)(F)H$ (4-F). To unambiguously characterize our type of compounds as being 16e and not 18-electron (18e), the hydride fluoride $Ru(IMes)_2(CO)(F)H$ (**4-F**) was prepared; it is reasonable to argue that the 18e *trans*-dihydride hydrogen fluoride $Ru(IMes)_2(CO)(HF)H_2$ complex would be unlikely given that no transition metal HF complexes have yet been fully characterized.[15] Complex **4-F** was prepared by addition of $Et_3N\cdot 3HF$ to $Ru(IMes)_2(AsPh_3)(CO)H_2$ (Scheme 3).[16,17] The hydride fluoride **4-F** displayed two distinctive NMR signals: a broad ^{19}F signal at −208.3 ppm and a high-field proton resonance at δ −24.55 (cf. **4-OH**, δ −23.15).

Structural characterization of **4-F** by X-ray crystallography was not definitive, insofar as location of the hydride ligand was not reliable (Figure 2, Table 1). The *trans* arrangement of the IMes ligands is close to linear (C(1)−Ru−C(22) = 176.31-(10)°) with the two five-membered imidazole rings of the carbenes twisted 47.3° from coplanarity. The model attained

(10) We would like to thank Professor Ged Parkin for alerting us to this possibility.

(11) Selected NMR data for **4-OH**: ^{13}C (C_6D_6, 298 K): δ 206.1 (d, $^2J_{C-H}$ = 13.9 Hz, Ru-*C*O), 198.0 (d, $^2J_{C-H}$ = 6.6 Hz, Ru-*C*(IMes)). **4-OEt**: ^{13}C (C_6D_6, 298 K): δ 205.12 (d, $^2J_{C-H}$ = 13.0 Hz, Ru-*C*O), 197.6 (d, $^2J_{C-H}$ = 6.1 Hz, Ru-*C*(IMes)). **4-SH**: ^{13}C (C_6D_6, 298 K): δ 202.6 (d, $^2J_{C-H}$ = 11.6 Hz, Ru-*C*O), 198.0 (br s, Ru-*C*(IMes)).

(12) High-field hydride resonances have been reported in some of the few, well-characterized *trans*-dihydride complexes (e.g., Rybtchinski, B.; Ben-David, Y.; Milstein, D. *Organometallics* **1997**, *16*, 3786), although much lower field signals have been reported in 18-electron *trans*-dihydride complexes of Ru(II). (a) Abdur-Rashid, K.; Clapham, S. E.; Hadzovic, A.; Harvey, J. N.; Lough, A. J.; Morris, R. H. *J. Am. Chem. Soc.* **2002**, *124*, 15104. (b) Li, T.; Churland, R.; Lough, A. J.; Abdur-Rashid, K.; Morris, R. H. *Organometallics* **2004**, *23*, 6239. (c) Abbel, R.; Abdur-Rashid, K.; Faatz, M.; Hadzovic, A.; Lough, A. J.; Morris, R. H. *J. Am. Chem. Soc.* **2005**, *127*, 1870.

(13) For representative examples, see: (a) Esteruelas, M. A.; Werner, H. *J. Organomet. Chem.* **1986**, *303*, 221. (b) Poulton, J. T.; Sigalas, M. P.; Eisenstein, O.; Caulton, K. G. *Inorg. Chem.* **1993**, *32*, 5490. (c) Poulton, J. T.; Sigalas, M. P.; Folting K.; Streib, W. E.; Eisenstein, O.; Caulton, K. G. *Inorg. Chem.* **1994**, *33*, 1476. (d) Buil, M. L.; Elipe, S.; Esteruelas, M. A.; Oñate, E.; Peinado, E.; Ruiz, N. *Organometallics* **1997**, *16*, 5748. (e) Edwards, A. J.; Elipe, S.; Esteruelas, M. A.; Lahoz, F. J.; Oro, L. A.; Valero, C. *Organometallics* **1997**, *16*, 3828. (f) Lee, H. M.; Smith, D. C., Jr.; He, Z.; Stevens, E. D.; Yi, C. S.; Nolan, S. P. *Organometallics* **2001**, *20*, 794.

(14) Heyn, R. H.; Macgregor, S. A.; Nadasdi, T. T.; Ogasawara, M.; Eisenstein, O.; Caulton, K. G. *Inorg. Chim. Acta* **1997**, *259*, 5.

(15) A hydrogen fluoride complex of iridium has been detected spectroscopically, but not structurally verified. (a) Patel, B. P.; Crabtree, R. H. *J. Am. Chem. Soc.* **1996**, *118*, 13105. (b) Lee, D.-H.; Kwon, H. J.; Patel, B. P.; Liable-Sands, L. M.; Rheingold, A. L.; Crabtree, R. H. *Organometallics* **1999**, *18*, 1615.

(16) Triethylamine trihydrofluoride ($Et_3N\cdot 3HF$ or TREAT-HF) has been used to prepare a number of late metal fluoride and bifluoride complexes in recent years. (a) Fraser, S. L.; Antipin, M. Yu.; Kroustalyov, V. N.; Grushin, V. V. *J. Am. Chem. Soc.* **1997**, *119*, 4769. (b) Whittlesey, M. K.; Perutz, R. N.; Greener, B.; Moore, M. F. *Chem. Commun.* **1997**, 187. (c) Jasim, N. A.; Perutz, R. N. *J. Am. Chem. Soc.* **2000**, *122*, 8685. (d) Braun, T.; Noveski, D.; Neumann, B.; Stammler, H.-G. *Angew. Chem., Int. Ed.* **2002**, *41*, 2745. (e) Grushin, V. V.; Marshall, W. J. *J. Am. Chem. Soc.* **2004**, *126*, 3068. (f) Vicente, J.; Gil-Rubio, J.; Bautista, D.; Sironi, A.; Masciocchi, N. *Inorg. Chem.* **2004**, *43*, 5665. (g) Grushin, V. V.; Marshall, W. J. *Organometallics* **2004**, *23*, 3343.

(17) $Ru(IMes)_2(CO)(F)H$ is formed in excellent yield upon C−F bond activation of either C_6F_6 or $CF_3CF{=}CF_2$ by $Ru(IMes)_2(CO)(OH)H$. Chatwin, S. L.; Jazzar, R. F. R.; Whittlesey, M. K., unpublished results.

Scheme 3

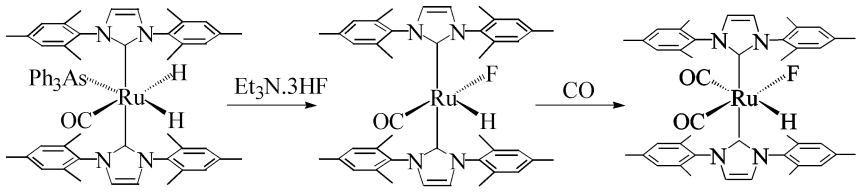

1 **4-F** **5-F**

Table 1. Selected Bond Lengths [Å] and Angles [deg] for Ru(IMes)$_2$(CO)(F)H (4-F)

	X-ray data	neutron data		X-ray data	neutron data
Ru(1)−C(1)	2.065(2)	2.069(5)	Ru(1)−F(1)	2.0326(15)	2.042(6)
Ru(1)−C(22)	2.071(2)	2.069(5)	O(1)−C(1A)	1.175(4)	1.160(8)
Ru(1)−C(1A)	1.781(3)	1.787(6)			
C(1)−Ru(1)−C(22)	176.31(10)	176.1(3)	C(1A)−Ru(1)−C(1)	92.69(11)	93.1(2)
F(1)−Ru(1)−C(1)	86.70(8)	87.0(2)	C(1A)−Ru(1)−C(22)	90.86(11)	90.5(2)
F(1)−Ru(1)−C(22)	89.82(8)	89.5(2)	C(1A)−Ru(1)−F(1)	175.99(11)	177.0(4)

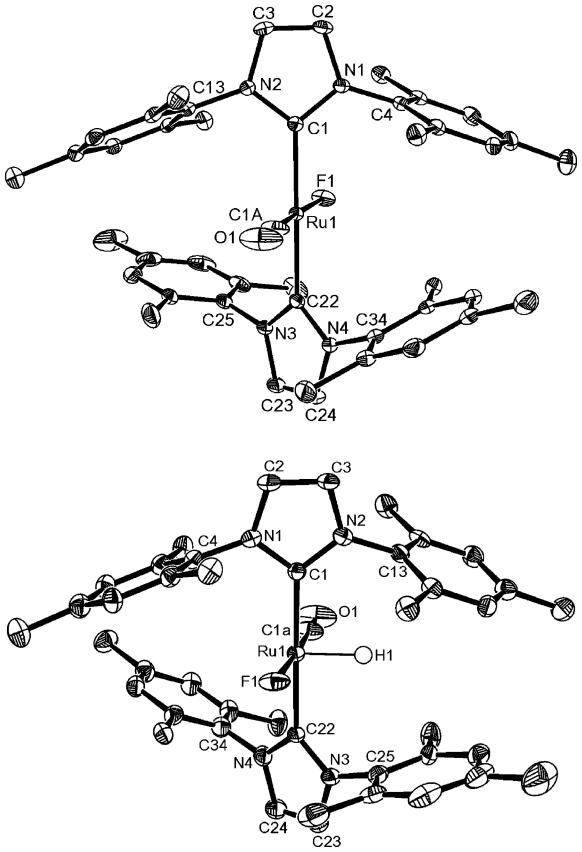

Figure 2. X-ray (top) and neutron (bottom) molecular structures of Ru(IMes)$_2$(CO)(F)H (**4-F**). Ellipsoids represented at 30% probability.

from the X-ray structure formed the basis for neutron data structural assignment, which revealed that the hydride ligand was, in fact, disordered over the two available sites in a 62:38 ratio (Figure 2, Table 1).

When **4-F** was placed under 1 atm CO at room temperature, the 18e dicarbonyl complex Ru(IMes)$_2$(CO)$_2$(F)H (**5-F**) was formed in the time of mixing, as evidenced by a color change from orange to colorless (Scheme 3). This 18e hydride fluoride complex displayed a doublet hydride resonance in the ^{1}H NMR spectrum at δ −3.80 (J_{HF} = 6.4 Hz), which showed an additional 46.3 Hz coupling upon incorporation of ^{13}CO *trans* to Ru-H. In line with other closely related 18e ruthenium(II) fluoride complexes, **5-F** displayed a very high field Ru-F resonance at

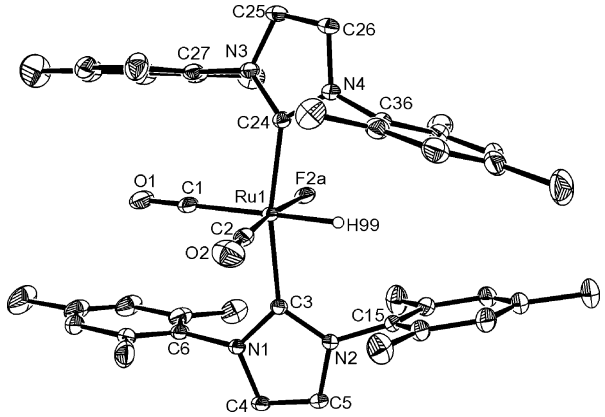

Figure 3. Molecular structure of Ru(IMes)$_2$(CO)$_2$(F)H (**5-F**). Ellipsoids represented at 30% probability.

Table 2. Selected Bond Lengths [Å] and Angles [deg] for Ru(IMes)$_2$(CO)$_2$(F)H (5-F)

Ru(1)−C(1)	1.988(2)	Ru(1)−F(2A)	2.019(5)
Ru(1)−C(2)	1.890(6)	O(1)−C(1)	1.130(3)
Ru(1)−C(3)	2.0998(15)	O(2)−C(2)	1.115(8)
Ru(1)−C(24)	2.1074(16)		
C(1)−Ru(1)−C(2)	96.14(18)	C(1)−Ru(1)−F(2A)	90.03(15)
C(2)−Ru(1)−C(3)	88.06(17)	C(2)−Ru(1)−F(2A)	173.4(2)
C(1)−Ru(1)−C(3)	96.33(7)	C(3)−Ru(1)−F(2A)	89.01(15)
C(2)−Ru(1)−C(24)	93.50(18)	C(24)−Ru(1)−F(2A)	88.12(15)
C(1)−Ru(1)−C(24)	95.66(7)	O(1)−C(1)−Ru(1)	177.5(3)
C(3)−Ru(1)−C(24)	167.67(6)	O(2)−C(2)−Ru(1)	177.6(2)

−379 ppm.[18] X-ray quality crystals of **5-F** were formed from a benzene/hexane solution. The coordination geometry at ruthenium is distorted from a regular octahedron (Figure 3, Table 2) with highly bent IMes−Ru−IMes and OC−Ru−CO angles (C(3)−Ru−C(24) 167.67(6)°, C(2)−Ru−C(1) 96.14(18)°). As expected, the two Ru−CO bond lengths exhibit significant differences (Ru−C(1) 1.988(2), Ru−C(2) 1.890(6) Å), the longer bond being opposite the more strongly *trans*-influencing hydride. The Ru−F distance of 2.019(5) Å is comparable to that found in *tcc*-Ru(PPh$_3$)$_2$(CO)$_2$F$_2$ (2.011(4) Å).[19]

(18) (a) Coleman, K. S.; Holloway, J. H.; Hope, E. G. *J. Chem. Soc., Dalton Trans.* **1997**, 1713. (b) Huang, D.; Koren, P. R.; Folting, K.; Davidson, E. R.; Caulton, K. G. *J. Am. Chem. Soc.* **2000**, *122*, 8916. (c) Kirkham, M. S.; Mahon, M. F.; Whittlesey, M. K. *Chem. Commun.* **2001**, 813.

(19) Brewer, S. A.; Coleman, K. S.; Fawcett, J.; Holloway, J. H.; Hope, E. G.; Russell, D. R., Watson, P. G. *J. Chem. Soc., Dalton Trans.* **1995**, 1073.

Scheme 4

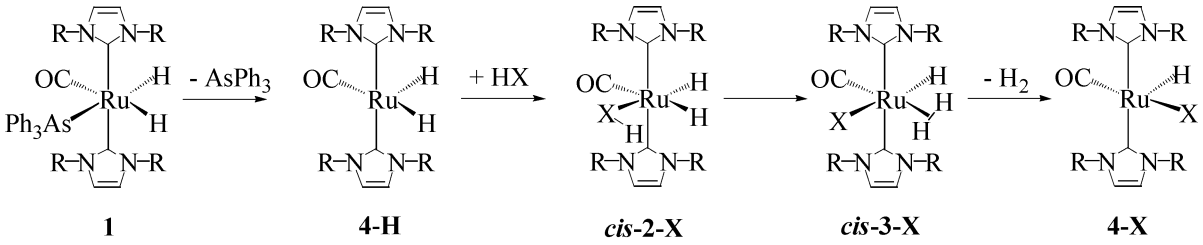

R = H (IH); R = mesityl (IMes)

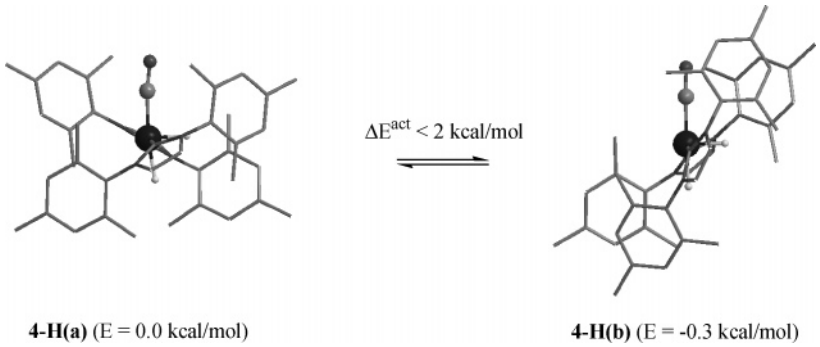

Figure 4. Top down representations of the alternative local minima located for **4-H**, highlighting the different orientations of the IMes ligands. IMes ligands are represented in wireframe with the ruthenium and the equatorial hydride and CO ligands shown in ball-and-stick form.

Computational Studies on the Formation of Ru(IMes)$_2$(CO)(X)H (4-X). A revised mechanism for the formation of these 16e species is shown in Scheme 4. Dissociation of $AsPh_3$ from *cis*-Ru(IMes)$_2$($AsPh_3$)(CO)H$_2$ (**1**) forms square-pyramidal Ru(IMes)$_2$(CO)H$_2$ (**4-H**), with a hydride in the axial position (referred to in the following as the T_H geometry). HX can then bind to give ***cis*-2-X**, which undergoes H-transfer to give a dihydrogen hydride intermediate (***cis*-3-X**).[8] Loss of dihydrogen followed by isomerization to place X *trans* to CO results in the observed 16e products.

As in our study of H-transfer in ***trans*-2-SH**, above, we have performed both full DFT (R = H) and QM/MM calculations (R = Mes) to model the reactivity of **4-H** with various HX species. Although the smaller IH model system proves useful in highlighting the main features of these reactions, several of the results obtained suggest that species combining IH and strongly basic heteroatom co-ligands, X, will be poor models for the IMes systems of interest here. First, as noted above, the presence of N−H···X H-bonding contributes to an overstabilization of any species featuring this interaction. Second, we found that computed Ru−X bond lengths in models of **4-X** (X = SH, OH, and F) were very dependent on the choice of NHC model ligand, being around 0.15 Å longer with IH than with IMes. Moreover, the IMes model gave good agreement with experimental Ru−X distances. The lengthening of the Ru−X bond in the IH models is probably driven by maximizing favorable N−H···X interactions. In addition such H-bonding should diminish the π-donor capacity of X, causing a reduction in X−Ru−CO "push−pull" effects that would normally shorten the Ru−X distance.[20] Finally, the steric bulk of the IMes ligand means that both H_2 loss from ***cis*-3-X** species and the subsequent isomerization of the {Ru(IR)$_2$(CO)(X)H} core are much more complicated (see below) than with the IH model, for which both processes proved to be barrierless. For these reasons[21] we report only the results obtained with QM/MM calculations when R = Mes, where the same partitioning scheme described above for the reactivity of ***trans*-2-SH** was employed.

For the reactant, **4-H**, two local minima were considered (Figure 4). The first of these, **4-H(a)**, was based on the solid-state structures of **4-F** with F replaced by H. Optimization of this structure produced the same staggered arrangement of the IMes ligands with respect to the Ru−H bond seen in **4-F**. However, this geometry would effectively block the approach of a sixth ligand toward the metal vacant site, which would become accessible only if the IMes ligands rotate out of the way. A second geometry was therefore generated, **4-H(b)**, based on a computed structure for the six-coordinate precursor, **1**. Upon removal of the $AsPh_3$ ligand, optimization produced the more open structure **4-H(b)** shown in Figure 4, where the IMes ligands approximately bisect the *cis*-OC−Ru−H angle. Test calculations on the rotation of the IMes ligands suggest interconversion between **4-H(a)** and **4-H(b)** would occur with a barrier of less than 2 kcal/mol. The more open form, **4-H(b)**, is also more stable (although by only 0.3 kcal/mol) and was thus used to represent the *cis*-Ru(IMes)$_2$(CO)H$_2$ moiety in all the subsequent reactivity studies.

X = SH. A minimum corresponding to the 18e adduct, ***cis*-2-SH**, was located with a long Ru−S distance of 2.51 Å *trans* to hydride, consistent with the relatively low H_2S binding energy of only 5.5 kcal/mol (Figure 5 gives key geometric data, while the computed reaction profiles for all X studied are given in Figure 6).[22] As with its *trans* isomer, H-transfer in ***cis*-2-SH** involves an elongation of the Ru−S distance (here to 2.68 Å) in order to orientate one S−H bond toward the accepting hydride ligand. The H-transfer transition state is similar to that derived from ***trans*-2-SH** and features a long H^H distance (2.03 Å) and effectively no change in the S−H distance (1.37 Å). This transition state leads directly to the dihydrogen complex ***cis*-3-**

(20) Caulton, K. G. *New J. Chem.* **1994**, *18*, 25.

(21) In certain cases use of IH also resulted in extra unexpected reactivity. For example, attempted optimization of the model species Ru(IH)$_2$(CO)(NH$_2$)(η^2-H$_2$)H led to deprotonation of one IH ligand.

(22) We also constructed energy profiles for the addition of H_2S and other HX species to **4-H(b)**. These showed there to be no significant barrier to HX addition.

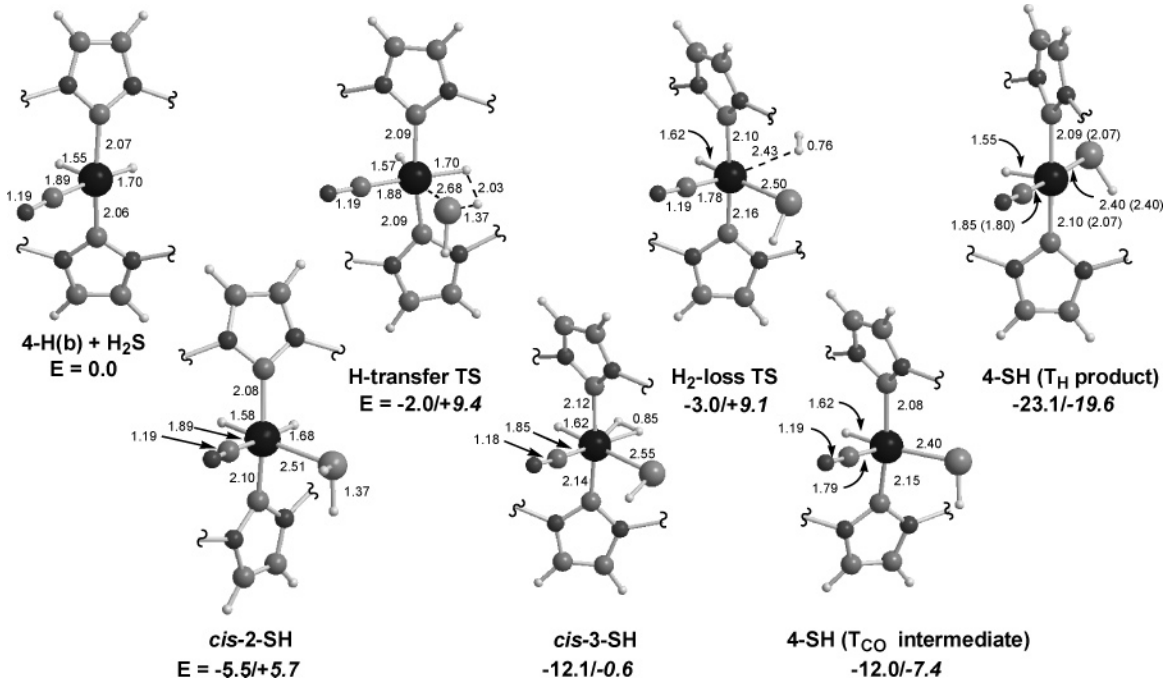

Figure 5. Computed stationary points (kcal/mol) for the reaction of **4-H** with H_2S. Selected key distances are given in Å and compared with experiment for **4-SH**. Computed relative free energies are included in italics. IMes ligands are truncated at the N−Mes bonds for clarity.

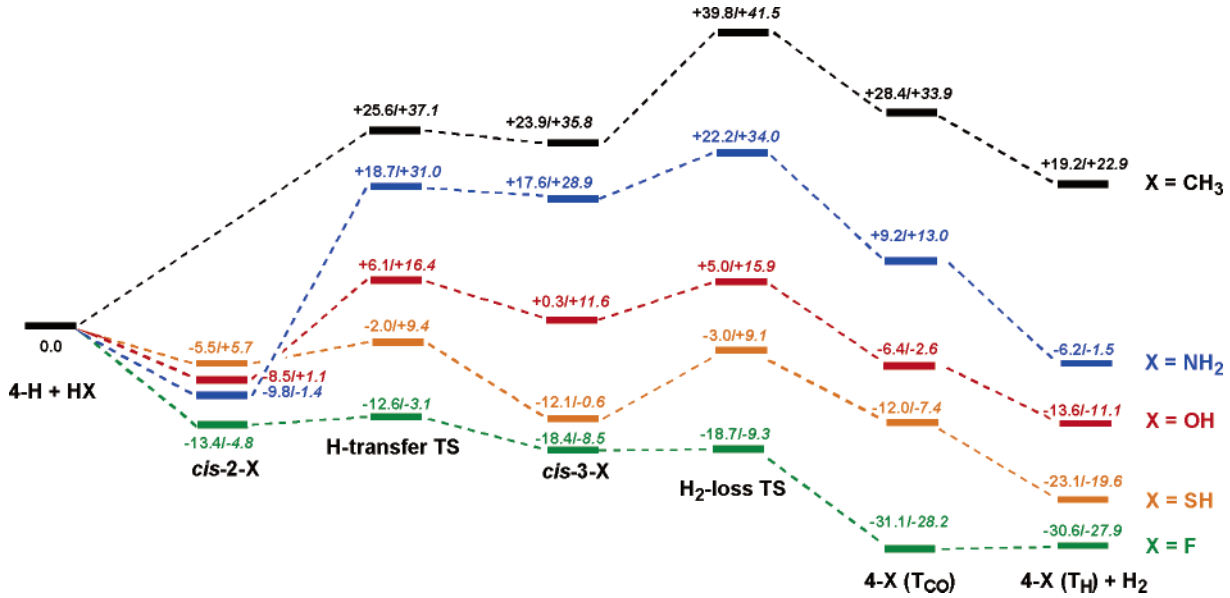

Figure 6. Computed reaction profiles (kcal/mol) for the reaction of **4-H** with HX (X = CH_3, NH_2, OH, SH, and F). Computed relative free energies are included in italics.

SH ($E = -12.1$ kcal/mol). The H-transfer step is computed to be downhill by 6.6 kcal/mol, compared to the value of 13.0 kcal/mol computed above for ***trans*-2-SH**. This difference probably arises from a more favorable arrangement of ligands in the product of the latter process, ***trans*-3-SH** having a π-donor, SH, *trans* to CO and an η^2-H_2 *trans* to hydride; in ***cis*-3-SH** SH is *trans* to hydride while the η^2-H_2 ligand is *trans* to CO. In contrast, the activation energy for the H-transfer step (3.5 kcal/mol) is slightly lower for ***cis*-2-SH**, possibly as the Ru−S bond that undergoes significant lengthening in this process is initially somewhat weaker in this species since the H_2S ligand is *trans* to hydride.

The loss of H_2 from ***cis*-3-SH** is complicated by the steric bulk of the IMes ligands and was studied via a linear transit constructed in terms of the distance between Ru and one H of the η^2-H_2 ligand. An H_2-loss transition state was thus located with a Ru···H distance of 2.43 Å and an Ru···H−H angle of 113°. Such an asymmetric geometry has previously been noted in the approach of H_2 toward other low-valent Ru centers.[23] Compared to ***cis*-3-SH**, this transition state exhibits a shorter Ru−S distance (2.50 Å, cf. 2.55 Å) and a wider OC−Ru−S angle (102.4°, cf. 90.2°). The barrier for H_2 loss from ***cis*-3-SH** is 9.1 kcal/mol, with the result that the H_2-loss transition state is only just lower in energy than that for H-transfer. The complete removal of H_2 results in only a partial isomerization

(23) Macgregor, S. A.; Eisenstein, O.; Whittlesey, M. K.; Perutz, R. N. *J. Chem. Soc., Dalton Trans.* **1998**, 291.

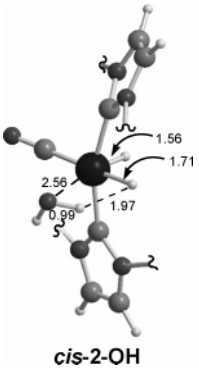

Figure 7. Computed structure for $Ru(IMes)_2(CO)H_2 \cdot H_2O$, ***cis*-2-OH**. Key distances are given in Å; the structure is truncated at the N−Mes bonds for clarity.

of the remaining {Ru(IMes)$_2$(CO)(SH)H} moiety, which forms a 16e intermediate with an approximate T_{CO} structure (OC−Ru−S = 113.5°). This intermediate owes its existence as a local minimum to the bulk of the IMes ligands, which effectively block the movement of the SH ligand. Isomerization to the final T_H form of Ru(IMes)$_2$(CO)(SH)H, **4-SH**, was modeled by rotating one IMes ligand relative to the other, which creates sufficient space for the OC−Ru−S angle to open to its final value of around 165°. The barrier associated with this final isomerization is estimated to be <1 kcal/mol, and as this process will therefore lie well below the highest point on the computed reaction profile (H-transfer), a full transition-state optimization was not attempted. The computed geometry of **4-SH** is in good agreement with that determined experimentally, and in particular, in light of the above discussion on the IH model systems, the Ru−S bond is well reproduced (see Figure 5).

X = OH or F. In general, the nature of the stationary points located for the reactions of H_2O and HF with **4-H** is similar to those described above for H_2S, and full details of all structures are given in the Supporting Information. One important difference, however, is that addition of H_2O or HF to **4-H** leads to the formation of dihydrogen-bound adducts, rather than ligation at the metal.[24] Thus, H_2O adds to give ***cis*-2-OH**, which is perhaps best formulated as $Ru(IMes)_2(CO)H_2 \cdot H_2O$, where one δ^+ hydrogen of water interacts with the δ^- hydride *trans* to CO (O−H···H−Ru = 1.97 Å; Ru···O = 2.56 Å, see Figure 7). H-transfer proceeds from this intermediate via the concerted addition of O−H over the Ru−H bond. The transition state for this step is more product-like than in the H_2S analogue, featuring a far greater degree of HX bond elongation (0.99 Å to 1.49 Å) and a much shorter H···H contact (0.91 Å). H-transfer is a less favorable process than in the H_2S case, as it involves both a higher activation barrier (14.6 kcal/mol) and the dihydrogen intermediate formed, Ru(IMes)$_2$(CO)(OH)(η^2-H$_2$)H (***cis*-3-OH**), is 8.8 kcal/mol less stable than $Ru(IMes)_2(CO)H_2 \cdot H_2O$ (see Figure 6).[9] Subsequent H_2 loss from ***cis*-3-OH** entailed a barrier of +4.7 kcal/mol and again resulted in only a partial isomerization of the remaining {Ru(IMes)$_2$(CO)(X)H} moiety to a T_{CO} form of **4-OH** (OC−Ru−O =132.1°). The final barrier for the T_{CO} to T_H isomerization of **4-OH** was estimated to be around 2 kcal/mol.

As with H_2O, HF also forms a dihydrogen-bound adduct with **4-H**. This species, $Ru(IMes)_2(CO)H_2 \cdot HF$, is apparently strongly bound (E = −13.4 kcal/mol) and exhibits a very short F−H···H−Ru distance of 1.34 Å. However, it also appears to lie in a very shallow local minimum, as the subsequent H-transfer proceeds with an activation barrier of only 0.8 kcal/mol to give Ru(IMes)$_2$(CO)(F)(η^2-H$_2$)H (***cis*-3-F**, E = −18.4 kcal/mol). The subsequent loss of H_2 also occurs with a minimal activation barrier (0.3 kcal/mol) and results in a more complete opening of the OC−Ru−X angle (to 163°) than was seen in the OH and SH analogues, probably reflecting the ease with which the smaller fluoride ligand can move between the two IMes ligands. The geometry of the 16e intermediate thus formed is very close to that optimized for **4-F** based on the crystal structure of this species, and the barrier associated with the movement of the IMes ligands to form this species was estimated to be ca. 2.3 kcal/mol.

X = NH_2 or CH_3. The above work models the observed reactions of H_2S, H_2O, and HF with **1**. However it is also of interest to investigate whether analogous reactivity may be accessible with other HX species such as NH_3 or CH_4. The reaction profiles computed with these species are included in Figure 6; as before, all relevant geometries are supplied as Supporting Information.

Ammonia forms a relatively stable ammine adduct with **4-H** (E = −9.8 kcal/mol) from which H-transfer entails an activation barrier of +28.5 kcal/mol via an extremely late transition state (N−H···H−Ru = 0.85 Å; N−H = 1.83 Å). H_2 loss from ***cis*-3-NH_2** is facile, with an activation barrier of only 4.6 kcal/mol; however, this process still represents the highest point on the reaction profile and corresponds to an overall activation barrier of 22.2 kcal/mol, relative to **4-H** and free NH_3. The reaction with NH_3 is therefore kinetically far more difficult than the equivalent reactions of H_2S, H_2O, or HF, although the 16e T_H product, Ru(IMes)$_2$(CO)(NH_2)H, **4-NH_2**, is reasonably stable (E = −6.2 kcal/mol).

With CH_4 no stable agostic complex could be located and the reaction is computed to proceed directly to an H-transfer transition state with an activation barrier of 25.6 kcal/mol. The dihydrogen intermediate, ***cis*-3-CH_3**, is also high in energy (E = +23.9 kcal/mol), but H_2 loss entails a significant additional barrier of 15.9 kcal/mol. The overall barrier relative to **4-H** and free CH_4 is therefore 39.8 kcal/mol. This, along with the energy of the T_H product, **4-CH_3** (+19.2 kcal/mol), suggests that C−H activation by the type of H-transfer process described here will be both kinetically and thermodynamically difficult.

The computed reaction profiles summarized in Figure 6 also report the free energies associated with each species (corrected to 298 K, in italics). As expected, entropy has the effect of destabilizing all the six-coordinate species. However, while accounting for this factor, the reaction with HF still proceeds without any overall barrier, while those with H_2S and H_2O have relatively small free energies of activation of +16.4 and +9.4 kcal/mol, respectively. In contrast, the analogous reactions of NH_3 and CH_4 are again far less favorable, proceeding with computed free activation barriers of +34.0 and +41.5 kcal/mol, respectively.

Discussion

The Ru(IMes)$_2$(CO)(X)H species described herein are the first members of a new family of unsaturated 16e Ru^{II} complexes similar to those M(PR$_3$)$_2$(CO)(X)H species developed by Caulton[13b,c] (M = Ru) and both Esteruelas[13d,e] and Werner[13a] (M = Os). Electronic factors such as X−Ru−CO push−pull interactions[20] and the presence of the high *trans*-influence hydride ligand in the apical site of the square-based pyramidal structure[14] have been cited as electronic reasons behind the

(24) Crabtree, R. H.; Siegbahn, P. E. M.; Eisenstein, O.; Rheingold, A. L. *Acc. Chem. Res.* **1996**, *29*, 348.

Table 3. Experimental[a] H−X Bond Dissociation Energies, $\Delta E_{cis\text{-}3\text{-}X}$, $\Delta E_{4\text{-}X}$ Values, and Relative Ru−X Bond Dissociation Energies in 4-X (computed, present study)

4-X	D_e(H−X)	$\Delta E_{cis-3-X}$	ΔE_{4-X}	relative D_e(Ru−X) in $Ru(IMes)_2(CO)(X)H$
X = H	104.2		0.0	0.0
X = CH_3	105.0	+23.4	+19.2	−18.4
X = NH_2	107.6	+17.6	−6.2	+9.6
X = OH	118.8	+0.3	−13.6	+27.1
X = F	136.3	−18.4	−30.6	+62.7
X = SiH_3	91.7	−8.7	−6.3	−6.2
X = PH_2	83.9	−3.2	−10.2	−10.1
X = SH	91.2	−12.1	−23.1	+10.1
X = Cl	103.2	−23.3	−34.2	+34.1
X = OEt	104.7	+4.7	−12.9	+13.4

[a] All H−X data come from: Blanksby, S. J.; Ellison, G. B. *Acc. Chem. Res*. **2003**, *36*, 255, and references therein, except that for PH_3; see: Berkowitz, J.; Ellison, G. B. Gutman, D. *J. Chem. Phys.* **1994**, *98*, 2744.

stability of such complexes. In addition, the use of bulky phosphines, PR_3, is essential for stability and the bulky IMes ligands appear to be playing a similar role in our systems.

Reaction Energetics. The data in Figure 6 show that the reaction of **4-H** with HX to give T_H **4-X** and H_2 becomes kinetically and thermodynamically more facile along the series CH_3 < NH_2 < OH < SH < F. The trend in overall exothermicity, ΔE_{4-X}, can be simply rationalized in terms of the strengths of the H−X bond broken and the Ru−X bond formed during these processes:

$$L_nRu{-}H + H{-}X \xrightarrow{\Delta E_{4-X}} L_nRu{-}X + H{-}H$$

$$\Delta E_{4-X} = -D_e(Ru{-}X) - D_e(H{-}H) + D_e(Ru{-}H) + D_e(H{-}X)$$

where D_e(Ru−X), for example, represents the homolytic bond dissociation energy of the Ru−X bond. D_e(Ru−X) can therefore be expressed as

$$D_e(Ru{-}X) = -\Delta E_{4-X} - D_e(H{-}H) + D_e(Ru{-}H) + D_e(H{-}X)$$

For X = H, $\Delta E_{4-X} = 0$, and so D_e(Ru−X) bond strengths can be calculated relative to D_e(Ru−H) according to

$$D_e(Ru{-}X) - D_e(Ru{-}H) = -\Delta E_{4-X} + D_e(H{-}X) - D_e(H{-}H)$$

where it is assumed that the strengths of the other Ru−L bonds are constant throughout.

Experimental literature values for D_e(H−X) and the resultant computed relative D_e(Ru−X) values are given in Table 3. These indicate that the H−X bond increases in strength from X = CH_3 to X = F by 31.3 kcal/mol; however this is more than compensated for by the strength of the Ru−X bond formed in the product, which increases by 81.1 kcal/mol along the same series. This relationship, indicating that the strongest substrate bond (here H−X) will be preferentially activated from a thermodynamic point of view, has been noted previously in many other systems.[25]

(25) (a) Jones, W. D.; Hessell, E. T. *J. Am. Chem. Soc*. **1993**, *115*, 554. (b) Bennett, J. L.; Wolczanski, P. T. *J. Am. Chem. Soc.* **1997**, *119*, 10696. (c) Holland, P. L.; Andersen, R. A.; Bergman, R. G.; Huang, J.; Nolan, S. P. *J. Am. Chem. Soc.* **1997**, *119*, 12800. (d) Wick, D. D.; Jones, W. D. *Organometallics* **1999**, *18*, 495. (e) Clot, E.; Besora, M.; Maseras, F.; Mégret, C.; Eisenstein, O.; Oelckers, B.; Perutz, R. N. *Chem. Commun.* **2003**, 490.

To assess a wider range of Ru−X bond strengths, we have extended our study by calculating ΔE_{4-X} for X = SiH_3, PH_2, Cl, and OEt. The resultant values for D_e(Ru−X) will be discussed in more detail below, but we note here that a slightly different pattern for ΔE_{4-X} is computed along the second-row species (SiH_3 > PH_2 < SH < Cl) and that this is mirrored in the same trend for both D_e(H−X) and D_e(Ru−X). With the exception of the CH_3/SiH_3 pair, D_e(Ru−X) is stronger for first-row X; however, this is counteracted for the group 15−17 species by the D_e(H−X) values which are always significantly lower for the second-row species. Overall, the trend in D_e(H−X) dominates, resulting in more favorable ΔE_{4-X} for second-row HX. For X = CH_3 vs SiH_3 both D_e(H−X) and D_e(Ru−X) combine to favor significantly the reaction with silane. Finally, for X = OH vs OEt, both D_e(H−X) and D_e(Ru−X) are weaker for X = OEt by ca. 14 kcal/mol, resulting in very similar ΔE_{4-X} for both water and ethanol.

The exothermicity of formation of the dihydrogen intermediates ***cis*-3-X** ($\Delta E_{cis-3-X}$) from **4-H** and HX also follows the same trends as noted above, namely, X = CH_3 < NH_2 < OH < F and X = SiH_3 > PH_2 < SH < Cl; in addition $\Delta E_{cis-3-X}$ is again always more favorable for a second-row HX species than for its first-row analogue. The similar computed results for ΔE_{4-X} and $\Delta E_{cis-3-X}$ suggest that the trends in D_e(Ru−X) will be the same in both systems. In principle, a similar analysis of D_e(Ru−X) in these 18e species could be performed using the approach described above for 16e **4-X**. However, in the 18e case, the assumption that all other ligand Ru−L bond strengths remain constant throughout breaks down, at least for the η^2-H_2 ligand (see below).

The computed barriers for the H-transfer step, relative to the combined energies of **4-H** and free HX, mirror the relative pK_a's of the HX substrates, as might be expected for a process involving an effective intermolecular protonation of a hydride ligand. H−X bond strengths apparently play little role in dictating the barriers for H-transfer, as the trend in D_e(H−X) strongly opposes that for the computed barriers. With the exception of CH_4, all HX form adducts prior to H-transfer, either directly to Ru (X = NH_2, SH) or to a hydride ligand via a dihydrogen interaction (X = OH or F). Adduct formation thus increases the activation barriers for the H-transfer step, and although the pK_a of HX still appears to determine the barrier height (i.e., X = F < SH < OH < NH_2), the relatively strong ammine adduct formed means that the barrier to H-transfer is actually higher for X = NH_2 than for X = CH_3.

Once formed, the ***cis*-3-X** species can either undergo a reversible H-transfer reaction to re-form ***cis*-2-X** or lose H_2 to afford **4-X**. For the relatively weakly basic ligands, X = F, OH, or SH, the back reaction entails reasonable barriers of 5.8, 5.8, and 10.1 kcal/mol, respectively. These, coupled to low thresholds for H_2 loss (F: +0.3 kcal/mol; OH: +4.7 kcal/mol; SH: +9.1 kcal/mol), mean that the onward reaction to **4-X** is kinetically preferential in these instances. With the more basic NH_2 and CH_3 ligands, low barriers for the reverse H-transfer are computed (<2 kcal/mol), and this process is kinetically preferred to H_2 loss. In general, the low barriers to H_2 loss computed for F, OH, and NH_2 (<5 kcal/mol) are consistent with a *cis*-labilization caused by these strong π-donor ligands. An intermediate barrier is computed with the weaker second-row π-donor SH (9.1 kcal/mol), while with X = CH_3 the barrier increases to 15.9 kcal/mol. Similar trends for the ease of ligand loss *cis* to a π-donor have been noted experimentally for both phosphine[26] and CO loss,[27] and for the latter this has been shown computationally to result from both a destabilization of the

ground state 18e complex and a π-stabilization of the resultant 16e species.[28]

Ru−X Relative Bond Strengths in Ru(IMes)$_2$(CO)(X)H Species. The computed relative Ru−X bond strengths in **4-X** can also be compared to those obtained experimentally for a range of different M−X-containing species based on either the measurement of exchange equilibria[29] or solution calorimetric studies.[30] Data for the type of parent M−X bonds investigated here are still relatively sparse, however, and in comparing with experimental results, it is important to take into account the effect of any substituent on X. For example M−NR$_2$ or M−OR bonds are significantly weaker when R = alkyl or aryl compared to R = H.[29b,31,32]

In general, our computed results for D_e(Ru−X) find good agreement with experiment, although no experimental study covers the full range of ligands studied here. There are several instances where low-valent M−OR bonds have been found to be stronger than analogous M−NR$_2$ bonds,[25c,29a−c,f] and in the one case where Ru−SH and Ru−OH relative bond strengths have been compared experimentally the latter was found to be stronger by at least 18.5 kcal/mol,[29a] compared with the 17 kcal/mol difference computed here. In Table 4 we compare our computed relative D_e(Ru−X) bond strengths for the **4-X** species with those obtained experimentally for Cp*Ru(PMe$_3$)$_2$X[29a] and Cp*$_2$ZrX$_2$.[30b] One key change upon going from saturated 18e Cp*Ru(PMe$_3$)$_2$X to unsaturated 16e **4-X** is a significant strengthening of the M−X bonds involving π-donors relative to the M−H bonds, by about 18 kcal/mol. A similar effect is seen in comparing Cp*Ru(PMe$_3$)$_2$X and Cp*$_2$ZrX$_2$, where the M−O/M−N bonds strengthen by about 27 kcal/mol relative to the M−H bond upon moving from saturated Ru to unsaturated Zr. In contrast, the difference between the M−H and M−Me bond strengths is approximately constant across all three systems; if anything, the M−Me bonds become relatively weaker in **4-X** and Cp*$_2$ZrX$_2$. These significant increases in the relative strengths of the M−X bonds involving π-donors in **4-X** and Cp*$_2$ZrX$_2$ presumably reflect the ability of these ligands to turn on X → M π-donation in these unsaturated systems, a possibility not available to hydride or alkyl ligands. Further evidence for this effect is seen by comparing M−H and M−Cl bond strengths. A number of studies involving saturated 18e Cp*Ru(CO)$_2$X,[30c] Cp$_2$Mo(X)$_2$,[33] CpMo(CO)$_3$X,[34] Cp*Ir(PMe$_3$)(X)$_2$,[30a] and Ir(PR$_3$)$_2$(CO)(Cl)(X)$_2$[35] systems indicate that the M−Cl bond is between 6 and 16 kcal/mol stronger than the M−H bond. In unsaturated **4-X** and Cp*$_2$ZrX$_2$ this difference rises to about 35 kcal/mol. In other studies very similar Rh−OD and Rh−D bond dissociation free energies of around 60 kcal/mol have been determined in [(TSPP)Rh(D$_2$O)X]$^{4-}$ species (TSPP = tetra-*p*-sulfonatophenylporphyrin), and this again presumably reflects the fact that these are formally saturated 18e Rh^{III} systems.[29e] Similarly, Ru−X bond dissociation energies in Ru(PMe$_3$)$_4$(H)(X) follow the trend X = H > OC$_6$H$_4$-*p*-Me > NHPh > CH$_2$Ph,[36] and the high relative strength of the Ru−H bond could well reflect both the saturated nature of the metal center in these species and the weakening effect of the aryl substituents.[31,32] Overall our analysis stresses the importance of considering both the nature of the metal center and the presence of any substituents on X when comparing relative M−X bond strengths.

Table 4. Computed and Experimental Relative Ru−X Bond Dissociation Energies

	Ru(IMes)$_2$(CO)(X)H	Cp*Ru(PMe$_3$)$_2$X[29a]	Cp*$_2$ZrX$_2$[30b] (average)
X = H	0.0	0.0	0.0
X = OH	+27.1	+8.9	+35.0
X = OR	+13.4 (R = Et)	−5.7 (R = Me)	+22.9 (R = CH$_2$CF$_3$)
X = NH$_2$	+9.6	−7.2[b]	+20.4[a]
X = R	−18.4 (R = Me)	−11.3 (R = CH$_2$COCH$_3$)	−13.3
X = SH	+10.1	> −9.6	
X = Cl	+34.1		+35.1

[a] Refers to the Zr−NH$_2$ bond in Cp*$_2$Zr(NH$_2$)(H). [b] Data relates to the experimental value determined for X = NHPh and includes a 14 kcal/mol correction for X = NH$_2$, based on the computational study of (DPPE)PtMe(X) systems in ref 32.

As mentioned above, trends in D_e(M−X) along the first- and second-row species are related to the trend in D_e(H−X). However, the D_e(M−X) values are clearly much more sensitive to the nature of X than D_e(H−X), and so it seems that the 1:1 correlation between M−X and H−X bond dissociation energies put forward for the saturated Cp*Ru(PMe$_3$)$_2$X system[29a] does not apply in the case of Ru(IMes)$_2$(CO)(X)H. Such deviations from the 1:1 relationship have been noted elsewhere,[25] and an explanation for this in terms of differential electrostatic interactions in H−X/M−X bonding has been put forward to account for this behavior.[25c] Such ionic contributions would also affect the Ru−X in the **4-X** series; however, it seems likely that M−X π-interactions dominate in these unsaturated systems, as this provides an extra bonding component to the M−X bond that is not possible for H−X bonds.

Reactivity. The computed reaction profiles for the formation of **4-X** species indicate a facile kinetic and favored thermodynamic process for X = OH, SH, and F, and this is consistent

(26) (a) Flood, T. C.; Lim, J. K.; Deming, M. A.; Keung, W. *Organometallics* **2000**, *19*, 1166. (b) Johnson, T. J.; Coan, P. S.; Caulton, K. G. *Inorg. Chem.* **1993**, *32*, 4594. (c) Bryndza, H. E.; Domaille, P. J.; Paciello, R. A.; Bercaw, J. E. *Organometallics* **1989**, *8*, 379.

(27) (a) Hoffman, N. W.; Prokopuk, N.; Robbins, M. J.; Jones, C. M.; Doherty, N. M. *Inorg. Chem.* **1991**, *30*, 4177. (b) Darensbourg, D. J.; Klausmeyer, K. K.; Reibenspies, J. H. *Inorg. Chem.* **1995**, *34*, 4933. (c) Darensbourg, D. J.; Klausmeyer, K. K.; Draper, J. D.; Chojnacki, J. A.; Reibenspies, J. H. *Inorg. Chim. Acta* **1998**, *270*, 405.

(28) Macgregor, S. A.; MacQueen, D. *Inorg. Chem.* **1999**, *38*, 4868. An explanation for the *cis*-labilization effect in terms of the varying electrostatic character of the metal center has also been put forward.[25c]

(29) (a) Bryndza, H. E.; Fong, L. K.; Paciello, R. A.; Tam, T.; Bercaw, J. E. *J. Am. Chem. Soc.* **1987**, *109*, 1444. (b) Erikson, T. K. G.; Bryan, J. C.; Mayer, J. M. *Organometallics* **1988**, *7*, 1930. (c) Hartwig, J. F.; Andersen, R. A.; Bergman, R. G. *Organometallics* **1991**, *10*, 1875. (d) Wicht, D. K.; Paisner, S. N.; Lew, B. M.; Glueck, D. S.; Yap, G. P. A.; Liable-Sands, L. M.; Rheingold, A. L.; Haar, C. M.; Nolan, S. P. *Organometallics* **1998**, *17*, 652. (e) Fu, X.; Wayland, B. B. *J. Am. Chem. Soc.* **2004**, *126*, 2623. (f) Eckert, N. A.; Smith, J. M.; Lachicotte, R. J.; Holland, P. L. *Inorg. Chem.* **2004**, *43*, 3306.

(30) (a) Nolan, S. P.; Hoff, C. D.; Stoutland, P. O.; Newman, L. J.; Buchanan, J. M.; Bergman, R. G.; Yang, G. K.; Peters, K. S. *J. Am. Chem. Soc.* **1987**, *109*, 3143. (b) Schrock, L. E.; Marks. *J. Am. Chem. Soc.* **1988**, *110*, 7701. (c) Luo, L.; Li, C.; Cucullo, M. E.; Nolan, S. P. *Organometallics* **1995**, *14*, 1333. (d) Huang, J. K.; Li, C. B.; Nolan, S. P.; Petersen, J. L. *Organometallics* **1998**, *17*, 3516.

(31) L$_n$M−OH bonds are typically about 15 kcal/mol stronger than L$_n$M−OR bonds (R = Me, Et),[29a/b,32] with L$_n$M−OPh bonds being at least 10 kcal/mol weaker still.[29b,32] Relative rhenium−amide bond strengths have been determined to be L$_n$Re−NH$_2$ (0.0) > L$_n$M−NHMe (−8.5 kcal/mol) > L$_n$M−NMe$_2$ (< −21.4 kcal/mol).[29b]

(32) Computed relative bond strengths for the (DPPE)PtMe(X) series reproduce the experimental trend well, provided the actual ligand used in the experimental study is employed. The Pt−N bond strength is computed to be 14 kcal/mol stronger with X = NH$_2$ compared to NHPh: Macgregor, S. A.; Neave, G. W.; Smith, C. *Faraday Discuss.* **2003**, *124*, 111.

(33) Calado, J. C. G.; Dias, A. R.; Salem, M. S.; Martinho-Simões, J. A. *J. Chem. Soc., Dalton Trans.* **1981**, 1174.

(34) Nolan, S. P.; López De La Vega, R.; Hoff, C. D. *J. Organomet. Chem.* **1986**, *315*, 187.

(35) Yoneda, G.; Blake, D. M. *Inorg. Chem.* **1981**, *20*, 67, and references therein.

(36) Hartwig, J. F.; Andersen, R. A.; Bergman, R. G. *Organometallics* **1991**, *10*, 1875.

with the formation of these **4-X** species observed experimentally. For X = NH_2, the equivalent reaction is thermodynamically accessible, although the large barrier to H-transfer may render this reaction kinetically blocked. Methane C−H bond activation by H-transfer to hydride appears unlikely from both the thermodynamic and kinetic viewpoints. Although the full reaction profiles for the remaining species (X = SiH_3, PH_2, and Cl) have not been constructed, the energies of the dihydrogen intermediates, ***cis*-3-X**, and the products, **4-X**, suggest that such species should be accessible and that the complete H-transfer process is therefore possible from the HX substrates. The lower pK_a's expected of the second-row HX species should also mean that barriers to H-transfer will be lower than those of their first-row equivalents. Indeed, **4-Cl** has already been synthesized, although not by an H-transfer process.[37]

Of the various H−X bond activation reactions discussed here, those for X = OH and NH_2 are perhaps of most interest, as these may form one step in a catalytic cycle for alkene hydration or hydroamination. The formation of **4-OH** has already been realized, and this species does exhibit insertion chemistry, although as yet this has not been observed with alkenes.[1a] As discussed above, the formation of **4-NH_2** via H-transfer with **4-H** may be problematic from a kinetic point of view. However, an alternative would be to consider an analogous H-transfer process with **4-Me**. Assuming **4-Me** can be synthesized by an alternative route (for example reaction of MeLi with **4-Cl**), the energetics of this process should strongly favor formation of the amide:

$$\textbf{4-Me} + \text{H-NH}_2 \xrightarrow{\Delta E = -25\ \text{kcal/mol}} \textbf{4-NH}_2 + \text{H-CH}_3$$

Such a process was considered recently by Cundari and Gunnoe for (PCP)Ru(CO)X systems (PCP = 2,6-(CH_2-P^tBu_2)$_2C_6H_3$).[38] They computed the N−H bond activation reaction of (PCP)Ru(CO)Me(NH_3) to give (PCP)Ru(CO)(NH_2) and CH_4 to be exothermic by 4 kcal/mol. Attempts to realize this process experimentally, however, were frustrated by intramolecular C−H activation processes. In our case, assuming the binding energy of NH_3 to **4-Me** is similar to that to **4-H** (ca. 10 kcal/mol), our calculations predict the equivalent reaction of Ru(IMes)$_2$(CO)(H)(Me)(NH_3) to give **4-NH_2** will be exothermic by ca. 15 kcal/mol. The process is therefore apparently more favorable than for the (PCP)Ru(CO)X system, although intramolecular C−H activation, well known for IMes ligands,[39] may well be a competing process in our systems as well. Finally, once **4-NH_2** is formed, alkene hydroamination could proceed by alkene insertion into the Ru−NH_2 bond to generate a β-aminoalkyl species. N−H bond activation via H-transfer over this Ru−alkyl bond would presumably have similarly favorable energetics as those derived above for **4-Me**. This process would release the hydroamination product, $CH_3CH_2NH_2$, and regenerate **4-NH_2**, thus completing the catalytic cycle. Efforts to realize this pathway are underway in our laboratories.

Conclusions

Density functional calculations have been used to model the reactions of *tcc*-Ru(IMes)$_2$($AsPh_3$)(CO)(H_2) with a variety of HX substrates. After $AsPh_3$/HX substitution, H−X bond activation via H-transfer to hydride is computed to be both readily accessible kinetically and favorable thermodynamically for X = SH, OH, and F. This led to the recharacterization of the products of these reactions as 16e T_H Ru(IMes)$_2$(CO)(X)H species. The equivalent reactions with NH_3 and CH_4 are computed to be far less favorable, although NH_3 activation by this method is predicted to be thermodynamically feasible. The reactions with second-row HX substrates are found to be more facile than those of their first-row congenors. These reactivity trends can be interpreted in terms of the HX pK_a, the H−X bond strength, and the Ru−X bond strength formed in the Ru(IMes)$_2$(CO)(X)H products. In these unsaturated species X → Ru π-donation plays an important role in strengthening Ru−X bonds relative to those Ru−X bonds involving non-π-donor ligands.

Experimental Section

General Comments. All manipulations were carried out using standard Schlenk, high-vacuum, and glovebox techniques. All solvents were distilled under a nitrogen atmosphere using standard routes. C_6D_6 and $C_6D_5CD_3$ (Aldrich) were vacuum transferred from potassium. CO (BOC, 99.9%) and ^{13}CO (Promochem, 99%) were used as received. Ru($AsPh_3$)$_3$(CO)H_2 and Ru(IMes)$_2$($AsPh_3$)(CO)H_2 were prepared according to the literature.[1a,40] IMes was prepared according to a modified route based on the method reported by Arduengo.[41] Proton NMR spectra were recorded on Bruker Avance 300 or 400 MHz NMR spectrometers and referenced to the chemical shifts of residual protio solvent resonances (C_6D_5H δ 7.15, $C_6D_5CD_2H$ δ 2.10). ^{13}C{^{1}H} NMR spectra were referenced to C_6D_6 (δ 128.0) and $C_6D_5CH_3$ (δ 21.1). ^{31}P{^{1}H} NMR chemical shifts were referenced externally to 85% H_3PO_4 (δ 0.0). ^{1}H COSY, ^{1}H−^{13}C HMQC, and HMBC experiments were performed using standard Bruker pulse sequences. IR spectra were recorded as Nujol mulls on a Nicolet Protégé 460 FTIR spectrometer. Elemental analyses were performed at the University of Bath.

Ru(IMes)(CO)(F)H (4-F). Triethylamine trihydrogen fluoride (Et_3N·3HF, 10 μL, 0.06 mmol) was added to a C_6D_6 solution (0.6 mL) of Ru(IMes)$_2$($AsPh_3$)(CO)H_2 (0.06 g, 0.057 mmol; prepared in situ from Ru($AsPh_3$)$_3$(CO)H_2 and IMes[1a]) and the resulting solution shaken vigorously for 5 min, during which the solution turned deep yellow-orange. The solution was concentrated under vacuum to 2 mL and layered with 10 mL of hexane to afford deep orange crystals of compound. Yield: 0.04 g, 92%. Analysis for $RuC_{43}H_{51}N_4OF$ [found (calcd)]: C, 67.9 (67.95); H, 6.40 (6.76); N, 7.33 (7.37). ^{1}H NMR (C_6D_6, 400 MHz, 293 K): δ 6.82 (br s, 4H, $C_6H_2Me_3$), 6.80 (br s, 4H, $C_6H_2Me_3$), 6.14 (s, 4H, CNC*H*=C*H*N), 2.33 (s, 12H, CH_3), 2.19 (s, 12H, CH_3), 2.04 (s, 12H, CH_3), −24.55 (s, 1H, Ru-H). ^{19}F NMR (C_6D_6, 293 K): −208.3 (br s, F-H). ^{13}C{^{1}H} (C_6D_6, 293 K): δ 206.3 (d, $^2J_{C-F}$ = 77.5 Hz, Ru-*C*O), 197.0 (d, $^2J_{C-F}$ = 6.1 Hz, Ru-*C*), 137.7 (s, N-*C*), 137.3 (s), 137.2 (s), 136.8 (s), 134.5 (s), 129.2 (s) 129.1 (s), 121.5 (s), 21.9 (s, CH_3), 18.9 (d, J = 4.2 Hz, CH_3), 18.7 (d, J = 5.0 Hz, CH_3). IR (cm^{-1}): 1873 (ν_{CO}).

Ru(IMes)$_2$(CO)$_2$(F)H (5-F). A benzene solution (5 mL) of **1** (0.20 g, 0.27 mmol) was stirred under 1 atm of CO for 30 min, during which time the color changed from pale orange to colorless followed by precipitation of a white powder. The solvent was

(37) Dissolution of **4-OH** in dichloromethane results in slow formation of **4-Cl**. Chatwin, S. L.; Jazzar, R. F. R.; Mahon, M. F.; Whittlesey, M. K., unpublished results.

(38) Conner, D.; Jayaprakesh, K. N.; Cundari, T. R.; Gunnoe, T. B. *Organometallics* **2004**, *23*, 2724.

(39) (a) Huang, J.; Stevens, E. D.; Nolan, S. P. *Organometallics* **2000**, *19*, 1194. (b) Jazzar, R. F. R.; Macgregor, S. A.; Mahon, M. F.; Richards, S. P.; Whittlesey, M. K. *J. Am. Chem. Soc.* **2002**, *124*, 4944. (c) Chilvers, M. J.; Jazzar, R. F. R.; Mahon, M. F.; Whittlesey, M. K. *Adv. Synth. Catal.* **2003**, *345*, 1111. (d) Trnka, T. M.; Morgan, J. P.; Sanford, M. S.; Wilhelm, T. E.; Scholl, M.; Choi, T.-L.; Deng, S.; Day, M. W.; Grubbs, R. H. *J. Am. Chem. Soc.* **2003**, *125*, 2546. (e) Abdur-Rashid, K.; Fedorkiw, T.; Lough, A. J.; Morris, R. H. *Organometallics* **2004**, *23*, 86.

(40) Harris, A. D.; Robinson, S. D. *Inorg. Chim. Acta* **1980**, *42*, 25.

(41) Arduengo, A. J., III; Dias, H. V. R.; Harlow, R. L.; Kline, M. *J. Am. Chem. Soc.* **1992**, *114*, 5530.

Table 5. Structural Details for 4-F and 5-F

	4-F (X-ray)	**4-F** (neutron)	**5-F**
molecular formula	$C_{43}H_{49}FN_4ORu$	$C_{43}H_{49}FN_4ORu$	$C_{44}H_{49}FN_4O_2Ru$
fw	757.93	757.93	785.94
T/K	150(2)	150(2)	150(2)
wavelength	0.71073	0.90000	0.71073
cryst syst	orthorhombic	orthorhombic	monoclinic
space group	*Pbca*	*Pbca*	$P2_1/a$
a/Å	17.0670(3)	17.0670(3)	18.6201(1)
b/Å	19.2300(5)	19.2300(5)	10.8135(1)
c/Å	23.1870(5)	23.1870(5)	20.8519(2)
β/deg			108.758(1)
U/Å^3	7609.9(3)	7609.9(3)	3975.49(6)
Z	8	8	4
D_c/g cm^{-3}	1.323	1.323	1.313
F(000)	3168	3168	1640
cryst size/mm	0.20 × 0.20 × 0.20	5.00 × 3.00 × 1.00	0.40 × 0.25 × 0.13
min., max. *θ*/deg	2.96, 27.48	5.23, 30.07	3.56, 30.02
index ranges	$-19 \le h \le 22$; $-13 \le k \le 24$; $-27 \le l \le 17$	$-18 \le h \le 18$; $-21 \le k \le 21$; $-25 \le l \le 24$	$-26 \le h \le 26$; $-14 \le k \le 15$; $-29 \le l \le 29$
no. of reflns collected	23 484	44 424	88 171
no. of indep reflns, *R*(int)	8383, 0.0452	4170, 0.2465	11 583, 0.0549
no. of reflns obsd [$I > 2\sigma(I)$]	5593	3224	9946
data completeness	0.962	0.759	0.996
absorp corr	none	wavelength-dependent absorp coeff	SORTAV
no. of data/restraints/params	8383/0/463	4170/0/891	11 583/1/514
goodness-of-fit on F^2	1.017	1.931	1.052
final R_1, wR_2 indices [$I > 2\sigma(I)$]	0.0374, 0.0796	0.1023, 0.1714	0.0364, 0.0922
R indices (all data)	0.0752, 0.0900	0.1471, 0.1782	0.0451, 0.0981
max., min. residual density/e Å^{-3}	0.492, −0.482	0.811, −0.943	1.550, −0.961

removed via cannula, and the precipitate washed with 2 × 5 mL of cold hexane. The solid was then dissolved in a minimum amount of toluene and layered with hexane (10 mL). Colorless crystals were isolated by filtration, washed with hexane (2 × 10 mL), and dried in vacuo. Yield: 0.19 g, 91%. Analysis for $RuC_{44}H_{49}N_4O_2F$ [found (calcd)]: C (67.24%) 67.35%, H (6.28%) 7.30%, N (7.13%) 7.45. ^{1}H NMR (C_6D_6, 400 MHz, 293 K): *δ* 6.75 (br s, 4H, $C_6H_2Me_3$), 6.72 (br s, 4H, $C_6H_2Me_3$), 6.07 (s, 4H, CNC*H*=C*H*N), 2.22 (s, 12H, CH_3), 2.16 (s, 12H, CH_3), 2.09 (s, 12H, CH_3), −3.80 (dd, $^2J_{H-13C}$ = 46.3 Hz, $^2J_{H-F}$ = 6.4 Hz, 1H, Ru-H). ^{19}F NMR (C_6D_6, 293 K): −379.5 (s, RuF). ^{13}C{^{1}H} (C_6D_6, 293 K): *δ* 205.0 (d, $^2J_{C-F}$ = 89.5 Hz, Ru-*C*O), 193.6 (d, $^2J_{C-F}$ = 9.6 Hz, Ru-*C*O), 187.8 (s, Ru-*C*), 139.5 (s, N-*C*), 137.7 (s), 137.4 (s), 136.8 (s), 129.4 (s), 122.7 (s), 21.8 (s, CH_3), 19.0 (s, CH_3), 18.9 (s, CH_3), 18.8 (s, CH_3), 18.7 (s, CH_3). IR (cm^{-1}): 1991 (ν_{CO}), 1930 (ν_{Ru-H}), 1880 (ν_{CO}).

Crystallography. Single crystals of compounds **4-F** and **5-F** were analyzed using a Nonius Kappa CCD diffractometer. Details of the data collections, solutions, and refinements are given in Table 5. The structures were both solved using SHELXS-97[42] and refined using full-matrix least squares in SHELXL-97.[42] The asymmetric unit in both structures was seen to contain one molecule of solvent (benzene) in addition to one molecule of the metal complex. The hydrogen atom attached to the metal center could not be reliably located in **4-F** and was therefore omitted from the refinement. In compound **5-F**, the hydride was readily located and refined at a distance of 1.6 Å from the ruthenium. The mutually *trans* fluorine and carbonyl ligands were also disordered in the latter structure (65:35 ratio). Convergence was otherwise uneventful in both cases.

The ambiguity regarding hydride location in **4-F** led us to investigate the structure of this compound by neutron diffraction. A rectangular crystal of dimensions 5 mm × 3 mm × 1 mm was wrapped in thin Al foil and glued to a standard sample pin with all face edges at large angles to the (vertical) rotation axis. The crystal was cooled to 150 K, and data were collected on the Very-Intense Vertical-Axis Laue Diffractometer (VIVALDI) at the Institut Laue-Langevin[43] (an earlier trial with another crystal showed that the reflections became very broad on cooling to 100 K and that the crystal had broken up on warming back to room temperature). Fourteen Laue diffraction patterns, each accumulated over 5 or 8 h, were collected at 20° intervals in a rotation of the crystal perpendicular to the incident beam. A total of 44 882 single, resolved reflections were recorded in the wavelength range 0.9−3.0 Å, of which 4173 were independent, corresponding to 76% of the complete unique set to d = 0.90 Å, the average minimum value of d observed over all patterns. The intensities were indexed and processed using the program LAUEGEN,[44] and the reflections were integrated and the background was removed using the program INTEGRATE+.[45] Each observation was corrected for absorption by the crystal, using the calculated wavelength-dependent absorption coefficient, $0.1048\lambda + 0.1107$ mm^{-1}, and for absorption of the diffracted beam through the cylindrical cryostat heat shields. The reflections were normalized to a common incident wavelength using the program LAUENORM.[46] Subsequent calculations for structure determination were carried out using the SHELXTL package. Initial H positions were obtained from the results of the earlier X-ray structure determination. The hydride ligand was readily located and seen to be disordered over two sites (H1, H1A) in a 62:38 ratio. Least-squares refinement of all atomic coordinates and anisotropic temperature factors for all atoms, with the exception of the disordered hydride moiety, resulted in a final agreement factor value, $R(1)$, of 10.23% for 4170 independent reflections with $I > 2\sigma(I)$. Since only the ratios between unit cell dimensions can be determined in the white-beam Laue technique, the dimensions found by X-ray diffraction were used in the neutron refinement; the observed ratios and angles were, however, in accord with the X-ray

(42) Sheldrick, G. M. *Acta Crystallogr.* **1990**, *467−473*, A46. Sheldrick, G. M. *SHELXL-97*, a computer program for crystal structure refinement; University of Göttingen, 1997.

(43) Wilkinson, C.; Cowan, J. A.; Myles, D. A. A.; Cipriani, F.; McIntyre, G. J. *Neutron News* **2002**, *13*, 37.

(44) (a) Campbell, J. W. *J. Appl. Crystallogr.* **1995**, *28*, 228. (b) Campbell, J. W.; Hao, Q.; Harding, M. M.; Nguti, N. D.; Wilkinson, C. J. *J. Appl. Crystallogr.* **1998**, *31*, 23.

(45) Wilkinson, C.; Khamis, H. W.; Stansfield., R. F. D.; McIntyre, G. J. *J. Appl. Crystallogr.* **1988**, *21*, 471.

(46) Campbell, J. W.; Habash, J.; Helliwell, J. R.; Moffat, K. *Q. Protein Crystallogr.* **1986**, *18*, 23.

values. Unit cell parameters for the neutron analysis (and their estimated standard deviations) were assumed to be the same as those for the X-ray analysis since both data sets were collected at the same temperature.

Crystallographic data for compounds **4-F** (X-ray), **4-F** (neutron), and **5-F** have been deposited with the Cambridge Crystallographic Data Centre as supplementary publications CCDC 271057−271059. Copies of the data can be obtained free of charge on application to CCDC, 12 Union Road, Cambridge CB2 1EZ, UK [fax: (+44) 1223 336033, e-mail: deposit@ccdc.cam.ac.uk].

Computational Details. All calculations employed the Gaussian 98 program.[47] With the smaller model systems incorporating the IH model ligand DFT calculations employed the BP86 functional with the Ru, Si, P, S, and Cl centers being described using the Stuttgart RECPs and the associated basis sets.[48] For the second-row atoms an extra set of d-orbital polarization functions was added ($\zeta^{Si} = 0.284$; $\zeta^{P} = 0.387$; $\zeta^{S} = 0.503$; $\zeta^{Cl} = 0.640$).[49] 6-31G** basis sets were used for C, N, O, and H atoms.[50] For models incorporating IMes ligands, QM/MM calculations were employed based on the partitioning approach shown in Scheme 2. The QM component of these calculations employed the same DF approach described above for the IH calculations, while the UFF was used for the MM components. For both full DFT and QM/MM calculations all stationary points were characterized by computation of the Hessian matrix to be either minima (all positive eigenvalues) or transition states (1 imaginary eigenvalue). Estimated transition-state geometries were initially produced from linear transits based on the H···H distance (for H-transfer) or Ru···H distance (H_2 loss). Full DFT transition states were further characterized by IRC calculations, which in all cases led to the expected local minima. For the QM/MM results IRC calculations are not available in Gaussian 98, and so the nature of the minima linked by a given transition state was confirmed by optimization of appropriate geometries generated from the linear transit studies. All energies include a correction for zero-point energies, and the free energies incorporate temperature and entropic effects corrected to 298.15 K.

Acknowledgment. We would like to thank Professor Ged Parkin (Columbia University) for valuable insight and helpful discussions. We acknowledge EPSRC, Heriot-Watt, and Bath University for financial support and Johnson Matthey plc for the loan of $RuCl_3$. Some of the computational studies in this paper were performed on the HP/COMPAQ ES40 multiprocessor cluster (Columbus) at the Rutherford Appleton Laboratory (RAL), and the provision of this facility by the EPSRC National Service for Computational Chemistry Software is gratefully acknowledged.

Supporting Information Available: X-ray crystallographic data including tables of atomic coordinates, bond lengths and angles, anisotropic displacement parameters, hydrogen coordinates and U_{eq}, and packing diagrams. This material is available free of charge via the Internet at http://pubs.acs.org.

OM0507427

(47) Frisch, M. J.; Trucks, G. W.; Schlegel, H. B.; Scuseria, G. E.; Robb, M. A.; Cheeseman, J. R.; Zakrzewski, V. G.; Montgomery, J. A., Jr.; Stratmann, R. E.; Burant, J. C.; Dapprich, S.; Millam, J. M.; Daniels, A. D.; Kudin, K. N.; Strain, M. C.; Farkas, O.; Tomasi, J.; Barone, V.; Cossi, M.; Cammi, R.; Mennucci, B.; Pomelli, C.; Adamo, C.; Clifford, S.; Ochterski, J.; Petersson, G. A.; Ayala, P. Y.; Cui, Q.; Morokuma, K.; Rega, N.; Salvador, P.; Dannenberg, J. J.; Malick, D. K.; Rabuck, A. D.; Raghavachari, K.; Foresman, J. B.; Cioslowski, J.; Ortiz, J. V.; Baboul, A. G.; Stefanov, B. B.; Liu, G.; Liashenko, A.; Piskorz, P.; Komaromi, I.; Gomperts, R.; Martin, R. L.; Fox, D. J.; Keith, T.; Al-Laham, M. A.; Peng, C. Y.; Nanayakkara, A.; Challacombe, M.; Gill, P. M. W.; Johnson, B.; Chen, W.; Wong, M. W.; Andres, J. L.; Gonzalez, C.; Head-Gordon, M.; Replogle, E. S.; Pople, J. A. *Gaussian 98*, Revision A.11.4; Gaussian, Inc.: Pittsburgh, PA, 2001.

(48) Andrae, D.; Häusserman, U.; Dolg, M.; Stoll, H.; Preuss, H. *Theor. Chim. Acta* **1990**, *77*, 123.

(49) Höllwarth, A.; Böhme, M.; Dapprich, S.; Ehlers, A. W.; Gobbi, A.; Jonas, V.; Köhler, K. F.; Stegmann, R.; Veldkamp, A.; Frenking, G. *Chem. Phys. Lett*. **1993**, *208*, 237.

(50) (a) Hehre, W. J.; Ditchfield, R.; Pople, J. A. *J. Chem. Phys*. **1972**, *56*, 2257. (b) Hariharan, P. C.; Pople, J. A. *Theor. Chim. Acta* **1973**, *28*, 213.